The Astrophysical Journal, 635:1187–1191, 2005 December 20

SWIFT UVOT DETECTION OF GRB 050318

M. Still,[1,2] P. W. A. Roming,[3] K. O. Mason,[4] A. Blustin,[4] P. Boyd,[1,5] A. Breeveld,[4] P. Brown,[3] M. De Pasquale,[4] C. Gronwall,[3] S. T. Holland,[1,2] S. Hunsberger,[3] M. Ivanushkina,[2,6] C. James,[4] W. Landsman,[1] K. McGowan,[4] A. Morgan,[3] T. Poole,[4] S. Rosen,[4] P. Schady,[3,4] B. Zhang,[7] H. Krimm,[1,2] T. Sakamoto,[1] P. Giommi,[8] M. R. Goad,[9] V. Mangano,[10] K. Page,[9] M. Perri,[8] D. N. Burrows,[3] N. Gehrels,[1] and J. Nousek[3]

Received 2005 April 5; accepted 2005 September 2

ABSTRACT

We present observations of GRB 050318 by the Ultraviolet/Optical Telescope (UVOT) on board the *Swift* observatory. The data are the first detections of a gamma-ray burst (GRB) afterglow decay by the UVOT instrument, launched specifically to open a new window on these transient sources. We showcase UVOT's ability to provide multicolor photometry and the advantages of combining UVOT data with simultaneous and contemporaneous observations from the high-energy detectors on the *Swift* spacecraft. Multiple filters covering 1800–6000 Å reveal a red source with a spectral slope steeper than the simultaneous X-ray continuum. Spectral fits indicate that the UVOT colors are consistent with dust extinction by systems at $z = 1.2037$ and 1.4436, redshifts where absorption systems have been preidentified. However, the data can be most easily reproduced with models containing a foreground system of neutral gas redshifted by $z = 2.8 \pm 0.3$. For both of the above scenarios, spectral and decay slopes are, for the most part, consistent with fireball expansion into a uniform medium, provided a cooling break occurs between the energy ranges of the UVOT and *Swift*'s X-ray instrumentation.

Subject headings: astrometry — galaxies: distances and redshifts — gamma rays: bursts — shock waves — X-rays: individual (GRB 050318)

Online material: color figures

1. INTRODUCTION

The multi-instrument *Swift* observatory (Gehrels et al. 2004) was launched on 2004 November 20. It carries three science instruments: the wide-angle, hard X-ray Burst Alert Telescope (BAT; Barthelmy et al. 2005), which locates GRBs to within 3′ on the sky; the narrow-field X-Ray Telescope (XRT; Burrows et al. 2005); and the UVOT. Specifications of the UVOT are described in Roming et al. (2005). The UVOT instrument has a vital role in imaging the field containing the burst, minutes after a trigger, and reporting rapidly the afterglow location to $<1''$ accuracy via the GRB Coordinates Network (GCN). UVOT's subsequent role is to provide a relatively uniform sample of the afterglow decay. It is this subsequent role that we report on here, describing the first afterglow detected by UVOT in multiple colors, and monitoring the decay until 40 ks after the burst.

2. OBSERVATIONS

The *Swift* BAT made a 17 σ detection of GRB 050318 at 15:44:37 UT (Krimm et al. 2005a). Burst parameters revised from Krimm et al. (2005c) include a T_{90} burst duration of 32 ± 2 s, with a total fluence of 2.1×10^{-6} ergs cm^{-2} in the 15–350 keV band. Within this energy band we find evidence of spectral evolution across three peaks in the prompt emission light curve. Peak 1, between $T - 1$ s and $T + 5$ s (where T is the trigger time), is well fit by a simple power law with spectral index $\beta_{\rm BAT} = -1.1 \pm 0.2$ ($\chi^2 = 57$ for 57 degrees of freedom [dof]). All uncertainties in this paper are reported to a 90% confidence level, while spectral and temporal decay indices are provided with respect to flux density, e.g., $F_\nu \sim t^\alpha \nu^\beta$. The burst was quiet for the next 17 s, followed by two overlapping but resolved peaks. Peak 2 ($T + 22$–27 s) fits to a cutoff power law with $\beta_{\rm BAT} = -0.2 \pm 0.5$ and $E_p = 68^{+23}_{-10}$ keV ($\chi^2 = 66$ for 56 dof). The spectrum softens considerably during the third peak ($T + 27$–32 s) and is fit with $\beta_{\rm BAT} = 0.2 \pm 0.4$, where $E_p = 46 \pm 7$ keV. BAT event data were not recorded for the final 2 s of the burst. However, examination of the BAT rate data in four energy bands suggests continued spectral softening during this period.

The burst was located to within 3′ (90% containment) of R.A. = 49°.651, decl. = −46°.392 (J2000.0). This corresponds to a Galactic latitude of −55° with a local reddening of $E(B - V) = 0.018$ mag (Schlegel et al. 1998) and a H-equivalent Galactic column density of $N_{\rm H} = 2.8 \times 10^{20}$ cm^{-2} (Dickey & Lockman 1990). After a 54 minute delay for Earth occultation, *Swift* slewed so that the narrow-field instruments could monitor the target.

Within the first 100 s settled observation of the UVOT sequence, a $V = 17.8$ source was found 2.′6 from the BAT position (Fig. 1), with no counterpart in archival plates (McGowan et al.

[1] NASA/Goddard Space Flight Center, Greenbelt, MD 20771.
[2] Universities Space Research Association.
[3] Department of Astronomy and Astrophysics, Pennsylvania State University, 525 Davey Laboratory, University Park, PA 16802.
[4] Mullard Space Science Laboratory, University College London, Holmbury St. Mary, Dorking, RH5 6NT Surrey, UK.
[5] Joint Center for Astrophysics, University of Maryland, Baltimore County, 1000 Hilltop Circle, Baltimore, MD 21250.
[6] Department of Physics and Astronomy, Brigham Young University, N208 ESC, Provo, UT 84602.
[7] Department of Physics, University of Nevada, 4505 Maryland Parkway, Las Vegas, NV 89154.
[8] ASI Science Data Center, ESRIN, 00044 Frascati, Italy.
[9] Department of Physics and Astronomy, University of Leicester, Leicester LE1 7RH, UK.
[10] Osservatorio Astronomico di Roma, Sede di Monteporzio Catone, via di Frascati 33, Roma I-00040, Italy.

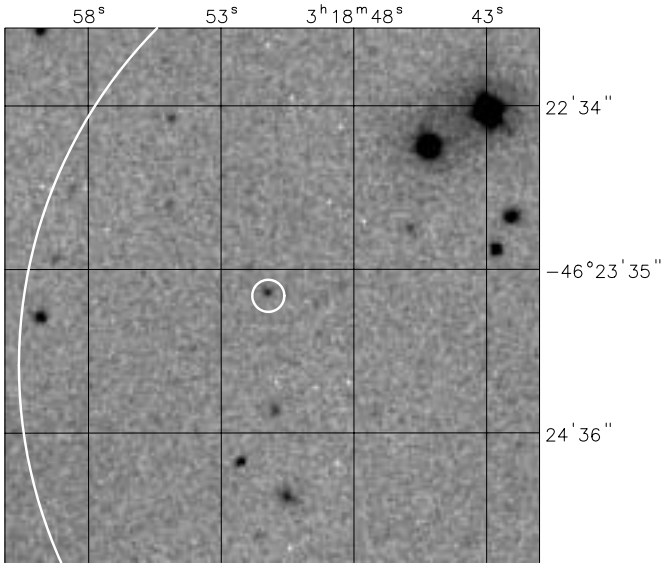

FIG. 1.—Stacked UVOT *V*-filter image of the field with the transient source at R.A. = 03h18m51s.15, decl. = −46°23′43.″7 (J2000.0), with the 3′ BAT error circle and the 6″ XRT error circle overlaid. Total exposure time for the stacked image is 3732 s. [*See the electronic edition of the Journal for a color version of this figure.*]

2005), consistent with the ground-based report of Mulchaey & Berger (2005). Subsequent exposures revealed a fading source 1.′1 from a transient X-ray counterpart (Markwardt et al. 2005; Nousek et al. 2005; Beardmore et al. 2005). A complete analysis and description of the XRT data reduction are reported in a separate paper (Perri et al. 2005). The UVOT position, as reported by De Pasquale et al. (2005), is R.A. = 03h18m51s.15, decl. = −46°23′43.″7 (J2000.0), with 0.″3 uncertainties.

UVOT completed 36 exposures before GRB 050319 triggered the BAT and became the new automated target (Krimm et al. 2005b). All detections of GRB 050318 $\geq 2\ \sigma$ above the background are tabulated in Table 1. AB filter magnitudes and background limits are based on in-orbit zero-point calibrations and differ from those used by McGowan et al. (2005) and De Pasquale et al. (2005), which were based on preflight calibrations and Vega magnitudes. The afterglow is not detected in UVW1 (centered at approximately 2500 Å), UVM2 (2200 Å), or UVW2 (1800 Å) light; the first settled exposures yield 3 σ upper limits of 19.3, 19.5, and 21.2 mag, respectively. Detections are made through the *U* (3500 Å), *B* (4400 Å), and *V* (5300 Å) filters in the range $T + 3200$–5400 s. On the next rotation of the filter wheel at $\sim T + 21{,}000$ s, the source has decayed below the 3 σ background

TABLE 1
UVOT DETECTIONS (> 2 σ ABOVE BACKGROUND) OF GRB 050318

T+ (s)	Exposure (s)	Filter	Magnitude	Significance (σ)
3230.....	100	*V*	$17.8^{+0.3}_{-0.2}$	5.1
3648.....	100	*U*	$19.6^{+0.3}_{-0.2}$	4.2
5382.....	880	*B*	$18.9^{+0.1}_{-0.1}$	19.6
11201.....	811	*V*	$19.1^{+0.2}_{-0.1}$	6.7
17041.....	707	*U*	$22.0^{+0.6}_{-0.4}$	2.3
22827.....	703	*V*	$19.5^{+0.3}_{-0.2}$	4.5
28609.....	712	*U*	$21.8^{+0.5}_{-0.3}$	2.8
40193.....	687	*U*	$22.1^{+0.8}_{-0.4}$	2.0

NOTES.—Mid-exposure times are relative to the trigger (*T*+), exposure durations, filters, AB magnitudes, and significance of the detection over background. Filter bandpasses are provided in Roming et al. (2005).

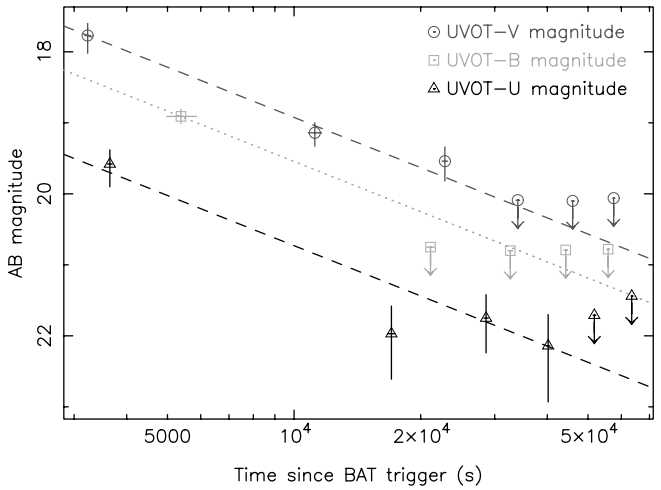

FIG. 2.—Plot of *U*, *B*, and *V* light curves of GRB 050318. The dashed lines are the best power-law fits to the *U* and *V* time series, α_{U+V}, excluding upper limits. The dotted line is an identical power-law model, renormalized to the first-epoch *B* magnitude. [*See the electronic edition of the Journal for a color version of this figure.*]

threshold in both the *U* and *B* bands. The magnitudes and detection significances at this epoch are $U = 21.9 \pm 0.5$, detected at 2.3 σ above background, and $B = 21.6 \pm 0.8$, 1.3 σ above background. The *V* source persists for three wheel rotations before fading below the background threshold in the range $T + 23{,}000$–34,000 s. The *U* band contains two further marginal source detections between 2–3 σ above background at $T + 28{,}609$ and $T + 40{,}193$ s.

2.1. *Source Decay*

All *U*, *B*, and *V* points, except the first 2 s *B* exposure, are plotted in Figure 2. Detections $\geq 2\ \sigma$ are provided with 90% confidence error bars, while all other points are given as upper limits at the 3 σ level. Using the first three *V* filter exposures, the power-law decay index for the *V* light curve is $\alpha_V = -0.87 \pm 0.24$ ($\chi^2 = 1.1$ for 1 dof). Assuming a power-law decay, the four *U*-band detections, $\geq 2\ \sigma$ above background, yield a consistent slope $\alpha_U = -1.00 \pm 0.25$ (90% confidence, $\chi^2 = 2$ for 2 dof). A weighted mean of the *U* and *V* decay slopes provides $\alpha_{U+V} = -0.94 \pm 0.17$, and the best fits to *U* and *V* data using this slope are plotted in Figure 2. A curve of the same slope is extrapolated to pass through the *B* detection at $T + 5382$ s. The XRT light curve at this epoch, presented by Perri et al. (2005), has a power-law decay index of $\alpha_{\rm XRT} = -1.2 \pm 0.1$. The probability that $\alpha_{\rm XRT}$ and α_{U+V} are identical is 8%.

Source detection in the $T + 21{,}105$ s *B* exposure is significant only to 1.3 σ and, using the *B* detection at $T + 5{,}382$ s as an anchor point, is inconsistent with the power-law decay index of α_{U+V} with 99.9% confidence. Either there is undersampled variability in the source, which provides us with a biased measure of the decay indices, or we are observing spectral evolution. Perhaps it is no coincidence that the next exposure after the second *B*-band observation is the one point on the *U* curve that is an outlier relative to the best-fit power-law decay index. It is inconsistent with α_{U+V} with 96% confidence. So short-timescale variability is perhaps the most plausible interpretation.

2.2. *Spectral Properties*

The two absorption systems at $z_1 = 1.2037$ and $z_2 = 1.4436$ reported by Berger et al. (2005) should produce Lyman systems redshifted into the UVM2 band. Assuming that consistent nondetections in filters blueward of a particular wavelength reveal

either dust or the Lyman limit of the host and its redshift, here we formally measure the spectral slope across the UVOT bands and search for a Lyman edge. All spectral models below include Galactic extinction appropriate for the source direction (see § 1), using the analytic formalism of Pei (1992) with $R_V = 3.08$. For simplicity, we assume that there is no Lyα forest in front of the host.

Using α_{U+V}, source rates in each filter were interpolated or extrapolated to a common epoch of $T + 4061$ s. Using the χ^2 fitting method outlined in Arnaud (1996) and references therein, a simple power-law model to all six points yields a fit with spectral index $\beta_{\rm UVOT} = -4.9 \pm 0.5$ and $\chi^2 = 24$ for 4 dof. The fit is poor statistically, and the index is steep compared to the 0.2–5 keV slope obtained from simultaneous XRT data of $\beta_{\rm XRT} = -1.1^{+0.2}_{-0.4}$ (§ 2.3). By adding an absorption edge to the power-law model, the quality of the fit improves to a statistically acceptable solution; $\beta_{\rm UVOT} = -2.4 \pm 1.5$ and, assuming the edge is due to the Lyman series, $z = 2.8 \pm 0.2$ ($\chi^2 = 1.0$ for 3 dof). The best-fit redshift is inconsistent with $z_2 = 1.4436$ (from Berger et al. 2005). For comparison, if z is forced to be 1.4436, the best fit yields $\beta_{\rm UVOT} = -4.5 \pm 1.5$ with $\chi^2 = 15$ for 4 dof. For completeness, fixing z at a value of 1.2037 yields $\beta_{\rm UVOT} = -4.5 \pm 0.5$ ($\chi^2 = 20$ for 4 dof).

We add host extinction to the model above, assuming a Small Magellanic Cloud (SMC) grain content with $R_V = 2.93$ (Pei 1992) and coupling the redshift of the dust to the neutral gas. The best solution yields $\beta_{\rm UVOT} = -1.0 \pm 5.0$, $z = 2.9 \pm 0.2$, and $E(B-V) < 0.26$ ($\chi^2 = 1.0$ for 2 dof); i.e., dust is not a necessary component for this model in order to provide a good description of the UVOT data. However, when the dust and gas are resituated at z_2, the fit does converge to an acceptable solution, provided we also include dust and gas at z_1, with $\chi^2 = 3.2$ for 2 dof, $\beta_{\rm UVOT} = +1.0 \pm 2.0$, $E(B-V)_1 = 0.4 \pm 0.2$, and $E(B-V)_2 < 0.27$, where $E(B-V)_1$ and $E(B-V)_2$ are the color excesses at z_1 and z_2, respectively. Consequently, gas and dust—at the redshifts of the two absorption systems reported by Berger et al. (2005) in front of a power-law continuum—provide an adequate fit to the UVOT data. However, the model containing a single gas and dust complex at the larger redshift of $z = 2.8 \pm 0.2$ provides the better fit.

Next we investigate whether the solutions above are biased by assuming an inappropriate temporal decay slope during the interpolation of UVOT data to a common epoch. For comparison, we repeat the previous exercise using the XRT decay index $\alpha_{\rm XRT} = -1.2$. Best-fit parameters and fit quality vary only a little compared to the previous analysis, and this results from the choice of a common epoch, which minimizes the systematic uncertainty in the interpolation. The best-fit solution without a dust component in the host (which does not formally improve the fit) is $\beta_{\rm UVOT} = -1.0 \pm 5.0$ and $z = 2.9 \pm 0.5$ ($\chi^2 = 1.0$ for 3 dof). The best fit with two dust and gas systems at z_1 and z_2 yields $\chi^2 = 2.6$ for 2 dof, $\beta_{\rm UVOT} = +1.0 \pm 4.1$, $E(B-V)_1 = 0.5 \pm 0.4$, and $E(B-V)_2 < 0.35$. Both solutions are identical to the previous analysis within uncertainties.

Intrinsic continuum slopes in the above models are poorly constrained due to a combination of low count rates and the relatively small spectral range of the filters. In §§ 2.3 and 3, by combining the UVOT data with a simultaneous XRT spectrum, we can place further constraints on the UVOT continuum, refine the redshift test and dust measurements, and compare a simple fireball model to the data.

2.3. *Spectral Energy Density*

Good XRT events have been extracted from within the time interval $T + 3180$–5822 s, which is the epoch between the start of the first V exposure and the end of the subsequent B detection, and binned by pulse height. The spectral fits below contain a core model of a floating power law, combined with fixed quantities for Galactic reddening and extinction in the local rest frame (see § 1). Galactic abundances are from Anders & Grevesse (1989). We use the 2005 April 5 empirical version of the XRT response calibration, which requires an additional absorption feature added to spectral models, corresponding to the neutral O K-feature at 0.54 keV, due to the optical filter.

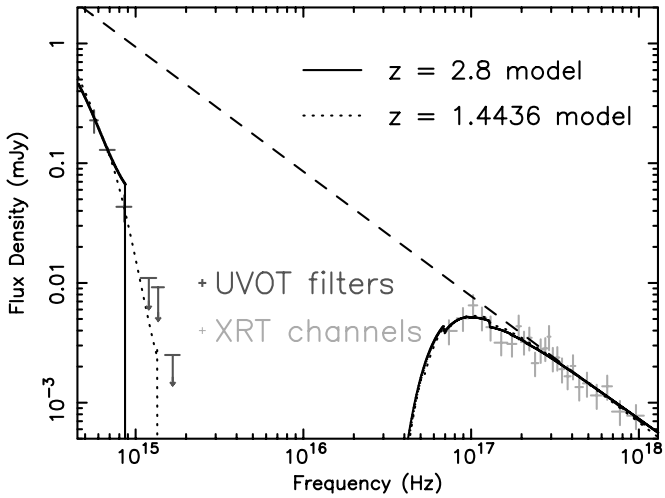

FIG. 3.—Combined UVOT and XRT spectrum of GRB 050318 at epoch $T +$ 4061 s, compared to two best-fit models, both containing a power-law model, reddened and absorbed by Galactic material. The solid line represents this model with an additional system of neutral gas and SMC-like dust at $z = 2.8$. The dotted line represents the model with two systems of neutral gas and SMC-like dust at $z_1 = 1.2037$ and $z_2 = 1.4436$. The dashed line is the best-fit intrinsic power-law spectrum. [*See the electronic edition of the Journal for a color version of this figure.*]

The best fit to the XRT data alone yields a power-law slope of $\beta_{\rm XRT} = -1.2 \pm 0.3$ and an integrated 0.2–5 keV flux of $(1.7 \pm 0.3) \times 10^{-11}$ ergs s^{-1} cm^{-2}. No extra spectral components are required with $\chi^2 = 10$ for 21 dof. On comparing the UVOT spectrum to the XRT spectral model, not only do we find an observed optical/UV spectral index much steeper than the X-ray continuum, but also the UV fluxes are >1 order of magnitude fainter than those predicted by the XRT model; therefore, the different slopes cannot be caused by a spectral break alone. A combined fit of the UVOT and XRT data to the core model yields a poor fit with a spectral index $\beta = -0.45 \pm 0.03$ and $\chi^2 = 506$ for 28 dof.

An acceptable combined fit of $\chi^2 = 13$ for 25 dof is obtained by adding SMC-like dust and neutral gas with Magellanic Cloud metallicities ($\langle {\rm H/Fe} \rangle = -0.5$) at one, free-floating redshift: $\beta = -1.0 \pm 0.1$, $z = 2.8 \pm 0.3$, $E(B-V) = 0.12 \pm 0.04$, and $\log N_{\rm H} < 2.0 \times 10^{21}$ cm^{-2}. The alternative model from § 2.2 replaces the $z = 2.8$ gas and dust with two systems at z_1 and z_2. Best-fit parameters are $\beta = -1.1 \pm 0.1$, $E(B-V)_1 = 0.23 \pm 0.12$, $E(B-V)_2 < 0.17$, $N_{\rm H1} < 1.7 \times 10^{21}$ cm^{-2}, and $N_{\rm H2} < 1.8 \times 10^{21}$ cm^{-2}, with $\chi^2 = 16$ for 24 dof. These two fits are plotted in Figure 3. Plotting the χ^2 landscape of this second model in the $E(B-V)_1$–$E(B-V)_2$ plane (Fig. 4) reveals that the majority of dust in this scenario is associated with the closer of the two systems at z_1.

In summary, model fits to the spectrum of GRB 050318 at $T + 4061$ s, where SMC-like neutral gas and dust are situated at z_1 and z_2 in front of a simple power-law source, reproduce the UVOT spectral index observed. The spectrum

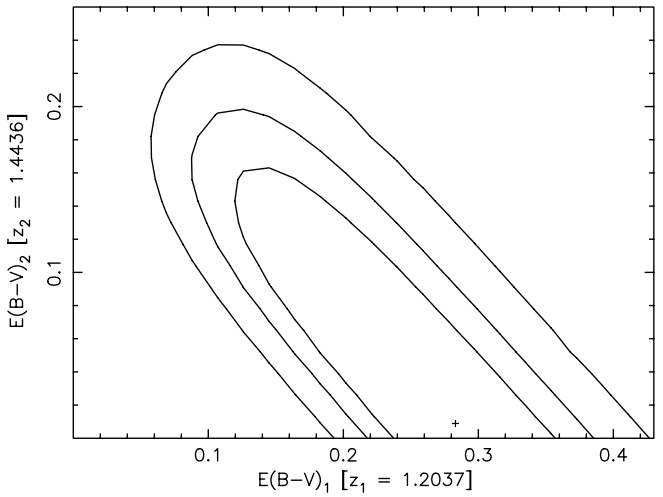

FIG. 4.—Confidence map in the $E(B-V)_1$–$E(B-V)_2$ plane. The two parameters represent the color correction, assuming $R_V = 2.93$, in two SMC-like dusty complexes at $z_1 = 1.2037$ and $z_2 = 1.4436$. Contours are 68%, 95%, and 99.7% confidence levels and indicate that a significant fraction of dust must reside in the closer of the two systems at z_1. [*See the electronic edition of the Journal for a color version of this figure.*]

is also well fit using a single system of gas and dust at $z = 2.8 \pm 0.3$.

3. DISCUSSION

3.1. *Dust and Gas Properties*

SMC dust has typically proved to be a good fit to extinction curves in GRB host galaxies (e.g., Jakobsson et al. 2004), as one might expect from a host containing a younger stellar population (Calzetti et al. 2000). The neutral column density within the host is poorly constrained, but by adopting the best-fit value from the SMC dust spectral model with $z = 2.8$, we find a gas to dust ratio of $N(\mathrm{H\ I})/A(V) < 7.6 \times 10^{21}$ cm^{-2} mag^{-1}, <50% of typical SMC lines of sight (Gordon et al. 2003). If we substitute the SMC dust with the Milky Way prescription of Pei (1992; $R_V = 3.08$) and assume solar metallicities in the neutral gas (Anders & Grevesse 1989), then the fit is also acceptable with $\chi^2 = 12$ for 25 dof, providing slightly different best-fit parameters of $\beta = -1.1 \pm 0.1$, $z = 2.4 \pm 0.5$, $E(B-V) = 0.28 \pm 0.13$, and $N_{\mathrm{H}} < 1.6 \times 10^{21}$ cm^{-2}. The gas to dust ratio for this case is $N(\mathrm{H\ I})/A(V) < 3.0 \times 10^{21}$ cm^{-2} mag^{-1}, consistent with the Galactic mean (Bohlin et al. 1978). Similarly, Large Magellanic Cloud (LMC) dust and gas properties with $R_V = 3.16$ (also from Pei 1992) yield $\beta = -1.0 \pm 0.1$, $z = 2.5 \pm 0.5$, $E(B-V) = 0.17 \pm 0.07$ and $N_{\mathrm{H}} < 3.2 \times 10^{21}$ cm^{-2}, with $\chi^2 = 13$ for 25 dof. In this case, $N(\mathrm{H\ I})/A(V) < 7.5 \times 10^{21}$ cm^{-2} mag^{-1}, which is consistent with the LMC sample from Gordon et al. (2003). This general model is therefore acceptable statistically for a range of dust and gas content.

A similar exercise applied to the alternative model, with extinction and absorption occurring at z_1 and z_2, yields a poor fit of $\chi^2 = 50$ for 24 dof when Milky Way dust and gas populations are assumed. Best-fit parameters are $\beta = -1.4 \pm 0.2$, $E(B-V)_1 = 0.28 \pm 0.10$, $E(B-V)_2 = 0.34 \pm 0.08$, $N_{\mathrm{H1}} < 2.0 \times 10^{21}$ cm^{-2}, and $N_{\mathrm{H2}} < 2.7 \times 10^{21}$ cm^{-2}. An LMC gas and dust model results in $\chi^2 = 18$ for 24 dof, where $\beta = -1.2 \pm 0.1$, $E(B-V)_1 = 0.25 \pm 0.15$, $E(B-V)_2 = 0.17 \pm 0.12$, $N_{\mathrm{H1}} < 3.2 \times 10^{21}$ cm^{-2}, and $N_{\mathrm{H2}} < 2.6 \times 10^{21}$ cm^{-2}. The gas to dust ratio, $N(\mathrm{H\ I})/A(V)$, for the LMC model is limited to $<5.0 \times 10^{21}$ mag^{-1} cm^{-2} in the system at z_2, which is a good candidate for the host galaxy; the same ratio for the SMC model is unconstrained. While SMC and LMC models provide acceptable fits, the Milky Way model does not, although we have made the simplifying assumptions that the dust contents of the two systems are identical and that a Lyα forest is absent in front of the burst. We also note that the constraint from § 2.3 that the majority of dust is located in the $z = 1.2037$ complex can be dropped if the extinction law in both systems is assumed to be featureless (e.g., Savaglio & Fall 2004), where $A(\lambda)/R_V = E(B-V)(5500\ \text{Å}/\lambda)^{\delta}$. In this scenario, an acceptable fit of $\chi^2 = 16$ for 23 dof is obtained, where $\beta = -1.1 \pm 0.1$, $E(B-V)_1 < 0.51$, $E(B-V)_2 < 0.46$, $\delta = 1.6^{+1.3}_{-0.8}$, $N_{\mathrm{H1}} < 6.4 \times 10^{20}$ cm^{-2}, and $N_{\mathrm{H2}} < 4.7 \times 10^{20}$ cm^{-2}.

3.2. *Interpretation*

The simplest afterglow emission model assumes synchrotron emission from a relativistic fireball, expanding into a uniform interstellar medium (Sari et al. 1998; Zhang & Mészáros 2004). Assuming that the injection break occurs at an energy <400 eV, the X-ray spectral slope of GRB 050318 indicates that $p = 2.4 \pm 0.2$, where $\beta = -p/2$, according to the parameterization of Sari et al. (1998). The simple fireball model then predicts that the temporal decay slope should have an index of $\alpha = (2-3p)/4 = -1.3 \pm 0.2$. This is consistent with the XRT decay index and the *B*-band lower limit, but comparison with the other optical bands is less convincing. The *U* and *V* indices are consistent with *p* with 14% and 3% confidences, respectively.

If we assume that the cooling break occurs at an energy greater than the injection break, and between the UVOT and XRT bandpasses, then the emission models predict $\alpha_{\mathrm{UVOT}} = 3(1-p)/4 = -1.05 \pm 0.2$. In this case, the *U* and *V* indices are consistent with *p*, with confidences of 80% and 36%, respectively. While the best spectral fit from § 2.3 does not formerly require a cooling break, it does not preclude it either. By replacing the model power-law continuum from § 2.3 with a broken power law of fixed spectral indices $\beta_{\mathrm{UVOT}} = -1.05$ and $\beta_{\mathrm{XRT}} = -1.2$, an acceptable fit is found using SMC dust with $\chi^2 = 13$ for 25 dof, $z = 2.9^{+0.3}_{-0.4}$, $E(B-V) = 0.15 \pm 0.02$, $\log N_{\mathrm{H}} = 19.9 \pm 1.5$ cm^{-2}, and providing a lower limit on the cooling break of $\nu_c > 4.8 \times 10^{15}$ Hz. The model with two dusty systems at z_1 and z_2 yields $\chi^2 = 16$ for 24 dof, $E(B-V)_1 = 0.23 \pm 0.12$, $E(B-V)_2 < 0.17$, $\log N_{\mathrm{H1}} < 21.1$ cm^{-2}, $\log N_{\mathrm{H2}} = 19.7 \pm 1.5$ cm^{-2}, and $\nu_c > 2.4 \times 10^{15}$ Hz. While the above model of a slow-cooling fireball within a uniform interstellar medium (ISM) fits most of the *Swift* data well in both redshift scenarios, the one caveat is the inconsistency between the *B* decay index limit and α_{U+V}.

Assuming that $z = 2.8$ is the host redshift and a cosmological model of $H_0 = 65$ km s^{-1} Mpc^{-1}, $\Omega_m = 0.3$, and $\Omega_\Lambda = 0.7$, the BAT 15–350 keV fluence yields an isotropic energy of $E_{\mathrm{iso}} = (3.6^{+0.7}_{-1.2}) \times 10^{52}$ ergs. Transforming a time-averaged value of $E_p = 49$ keV to the rest frame of the burst, we find $E'_p = 196^{+33}_{-51}$ keV [cf. $E_{\mathrm{iso}} = (1.4^{+0.2}_{-0.4}) \times 10^{52}$ ergs and $E'_p = 119^{+22}_{-35}$ keV at $z_2 = 1.4436$]. Since both redshifts yield spectral parameters consistent with the E_{iso}-E_p relationship derived by Amati et al. (2002), the BAT spectral analysis of this burst cannot provide useful diagnostics for testing the optical redshift candidates.

4. CONCLUSION

This paper reports the first significant optical detection of a GRB afterglow and subsequent monitoring of the decay by the UVOT instrument on board the *Swift* observatory. Compared to a simple power-law continuum model, the general deficit of UV emission can be for either using gas extinction at redshifts of $z_1 = 1.2037$ and $z_2 = 1.4426$, corresponding to the absorption

systems found by Berger et al. (2005), or using Lyman depletion from an object at $z = 2.8 \pm 0.3$, which would indicate that the two systems at z_1 and z_2 belong to foreground objects. Consequently, the UVOT data cannot unambiguously determine the host galaxy redshift for this burst. This will be a common occurrence when *Swift* does not detect a UV source. We note that there is no evidence for a $z = 2.8$ host galaxy in the 5000–7000 Å spectroscopy of Berger et al. (2005); however, hosts at this redshift have typically been identified by absorption features at bluer wavelengths, such as a damped Lyα line (Hjorth et al. 2003), which would occur at 4617 Å at $z = 2.8$. Since an identified absorption line provides only a lower limit to the host redshift, currently available evidence only allows a lower limit to be placed on the redshift of $z \geq 1.4436$. Decay curves and the UVOT/XRT spectral energy distribution reveal, for the most part, consistency with the picture of a slow-cooling fireball in a uniform ISM. However, the inferred steepness of the *B*-band decay slope, relative to *U* and *V*, may indicate some deviations from the simple model.

This work was sponsored at Penn State by NASA's Office of Space Science through contract NAS 5-00136, and at MSSL and Leicester by funding from PPARC. We gratefully acknowledge the contributions of all members of the *Swift* team.

REFERENCES

Amati, L., et al. 2002, A&A, 390, 81
Anders, E., & Grevesse, N. 1989, Geochim. Cosmochim. Acta, 53, 197
Arnaud, K. A. 1996, in ASP Conf. Ser. 101, Astronomical Data Analysis Software and Systems V, ed. G. Jacoby & J. Barnes (San Francisco: ASP), 17
Barthelmy, S., et al. 2005, Space Sci. Rev. 2005, in press (astro-ph/0507410)
Beardmore, A. P., et al. 2005, GCN Circ. 3133, http://gcn.gsfc.nasa.gov/gcn3/3133.gcn3
Berger, E., et al. 2005, ApJ, 634, 501
Bohlin, R. C., Savage, B. D., & Drake, J. F. 1978, ApJ, 224, 132
Burrows, D. N., et al. 2005, Space Sci. Rev., in press (astro-ph/0508071)
Calzetti, D., Armus, L., Bohlin, R. C., Kinney, A. L., Koornneef, J., & Storchi-Bergmann, T. 2000, ApJ, 533, 682
De Pasquale, M., et al. 2005, GCN Circ. 3123, http://gcn.gsfc.nasa.gov/gcn3/3123.gcn3
Dickey, J. M., & Lockman, F. J. 1990, ARA&A, 28, 215
Gehrels, N., et al. 2004, ApJ, 611, 1005
Gordon, K. D., Clayton, G. C., Misselt, K. A., Landolt, A. U., & Wolff, M. J. 2003, ApJ, 594, 279
Hjorth, J., et al. 2003, ApJ, 597, 699
Jakobsson, P., et al. 2004, A&A, 427, 785
Krimm, H. et al. 2005a, GCN Circ. 3111, http://gcn.gsfc.nasa.gov/gcn3/3111.gcn3
———. 2005b, GCN Circ. 3117, http://gcn.gsfc.nasa.gov/gcn3/3117.gcn3
———. 2005c, GCN Circ. 3134, http://gcn.gsfc.nasa.gov/gcn3/3134.gcn3
Markwardt, C., Boyd, P., Gehrels, G., Hurley, K., Marshall, F. E., & Still, M. 2005, GCN Circ. 3112, http://gcn.gsfc.nasa.gov/gcn3/3112.gcn3
McGowan, K., et al. 2005, GCN Circ. 3115, http://gcn.gsfc.nasa.gov/gcn3/3115.gcn3
Mulchaey, J., & Berger, E. 2005, GCN Circ. 3114, http://gcn.gsfc.nasa.gov/gcn3/3114.gcn3
Nousek, J. A., et al. 2005, GCN Circ. 3113, http://gcn.gsfc.nasa.gov/gcn3/3113.gcn3
Pei, Y. C. 1992, ApJ, 395, 130
Perri, M., et al. 2005, A&A, 442, L1
Roming, P. W. A., et al. 2005, Space Sci. Rev., in press (astro-ph/0507413)
Sari, R., Piran, T., & Naryan, R. 1998, ApJ, 497, L17
Savaglio, S., & Fall, S. M. 2004, ApJ, 614, 293
Schlegel, D. J., Finkbeiner, D. P., & Davis, M. 1998, ApJ, 500, 525
Zhang, B., & Mészáros, P. 2004, Int. J. Mod. Phys. A, 19, 2385